Supporting Information

Weakening Hydrogen Adsorption on Nickel via Interstitial Nitrogen Doping Promotes Bifunctional Hydrogen Electrocatalysis in Alkaline Solution

Tingting Wang,[1†] Miao Wang,[1†] Hao Yang,[1†] Mingquan Xu,[2] Chuandong Zuo,[3] Kun Feng,[1] Miao Xie,[1] Jun Deng,[1] Jun Zhong,[1] Wu Zhou,[2] Tao Cheng,[1*] and Yanguang Li[1*]

[1]Institute of Functional Nano and Soft Materials (FUNSOM), Jiangsu Key Laboratory for Carbon-Based Functional Materials and Devices, Soochow University, Suzhou 215123, China.

[2]School of Physical Sciences University of Chinese Academy of Sciences, Beijing, 100049 China.

[3]Beijing Key Laboratory of Opto-Electronic Functional Materials & Micro-Nano Devices, Department of Physics, Renmin University of China, Beijing, 100872, China.

[†]These authors contributed equally.

Email correspondence: tcheng@suda.edu.cn; yanguang@suda.edu.cn

Experimental Section:

Preparation of Ni-CP, np-Ni_3N and np-Ni.

In a typical synthesis, 0.6 mmol of $Ni(NO_3)_2 \cdot 6H_2O$ and 0.3 g polyvinylpyrrolidone (PVP) were dissolved in 20 mL of water to form solution A. 0.4 mmol of $K_2[Ni(CN)_4]$ was dissolved in 20 mL of water to form solution B. The two solutions were then mixed together under vigorous magnetic stirring, resulting in a solid precipitate with a light cyan color. After being aged at RT for 24 h, the precipitate was collected by centrifugation, repetitively washed with ethanol for five times and then with water for two times to remove excessive PVP, and lyophilized. It was named as Ni-CP. It was found that a small amount of PVP remained adsorbed on Ni-CP. For the second step, Ni-CP was annealed inside a tube furnace at 450 °C for 1 h under 10% NH_3/N_2 or Ar to form np-Ni_3N or np-Ni, respectively.

Material characterizations.

Scanning electron microscopy (SEM) images were carried out on the Supera 55 Zeiss scanning electron microscope. Transmission electron microscopy (TEM) images were taken on the FEI Tecnai F20 transmission electron microscope operating at an acceleration voltage of 200 kV. Fourier-transform infrared spectroscopy (FT-IR) spectra were collected on a Bruker Vertex 70v FT-IR spectrometer. Aberration-corrected STEM imaging and EELS mapping were performed on a Nion HERMES-100 under the accelerating voltage of 60 kV and 100 kV with the probe forming aperture of 30 mrad. Bright field (BF) and annular dark field (ADF) images were acquired simultaneously at the 32 mrad convergence angle. The EELS mapping was performed at the same setting with the collection angle of about 75 mrad. X-ray photoelectron spectroscopy (XPS) spectra were collected on the Ultra DLD XPS Spectrometer. X-ray diffraction (XRD) patterns were collected from the PANalytical X-ray diffractometer at a scan rate of 0.05^o/s. Thermogravimetric analysis (TGA) was

performed on the Mettler Toledo TGA/DSC1 thermogravimetric analyzer under air and nitrogen respectively from 25 °C to 800 °C with a ramping rate of 10 °C/min. Raman spectroscopy was performed on the Horiba Jobin-Yvon LabRam HR800 Raman spectrometer with a laser of 633 nm wavelength. Ni K-edge XANES and EXAFS spectra were collected at beamline 17C1, from ≈200 eV below to ≈300 eV above the Ni K-edge in the transmission mode with a step size of 0.25 eV in the near edge region and a dwell time of 2 s.

Electrochemical measurements

For rotating disk electrode (RDE) measurements, 1 mg of np-Ni_3N (or np-Ni) and 0.3 mg of Ketjenblack carbon were dispersed in 225 μL of ethanol and 8 μL of 5 wt% Nafion solution, and ultra-sonicated for 1 h to form a uniform catalyst ink. 10 μL (or 20 μL) of the catalyst ink was then dropcast onto the glassy carbon RDE electrode (area: 0.196 cm^2, from Pine Instruments) to form a smooth film with active material loading of 0.16 mg_{Ni3N}/cm^2 (or 0.32 mg_{Ni3N}/cm^2). 20 wt% Pt/C and 20 wt% PtRu/C (both purchased from Fuel Cell Store) were introduced as the reference. To prepare its working electrode, 1 mg of 20 wt% Pt/C (or 20 wt% PtRu/C) was dispersed in 500 μL of ethanol and 6 μL of 5 wt% Nafion solution, and ultra-sonicated for 40 min to form a uniform catalyst ink. 5 μL of the catalyst ink was then dropcast onto the RDE electrode to achieve active material loading of 10 $\mu g_{Pt}/cm^2$ (or 10 $\mu g_{Pt+Ru}/cm^2$). HOR RDE experiments were performed in a standard three-electrode system using the catalyst-loaded RDE as the working electrode, a saturated calomel electrode (SCE) as the reference electrode and a graphite rod as the counter electrode. All the potential readings were measured against SCE and reported against reversible hydrogen electrode (RHE). They were compensated for the ohmic loss. Prior to HOR measurements, the 0.1 M KOH electrolyte was bubbled with 99.999% H_2 for 30 min. Gentle H_2 bubbling was continued during HOR measurements to ensure the H_2 saturation of the

electrolyte. RDE polarization curves were collected at different electrode rotating speeds with a scan rate of 1 mV/s. Mass-specific kinetic current J_{mk} and mass-specific exchange current J_{m0} were calculated from the Koutecky–Levich and the Butler–Volmer equation according to previous reports.[1, 2] CO poisoning experiment was performed by suddenly introducing 5% CO to H_2-saturated 0.1 M KOH for 100 s while recording the chronoamperometric response of the working electrode biased at 0.05 V. HER measurements were carried out in 1 M KOH. The polarization curves were collected under N_2 at a scan rate of 10 mV/s.

Computational details

The DFT calculations were performed with the Vienna Ab initio Simulation Package (VASP) version 5.4.4,[3-5] using the generalized gradient approximation (GGA) of Perdew, Burke, and Ernzerhof (PBE) flavor[6] of density functional theory (DFT) and the projector augmented wave (PAW) method to account for core-valence interactions. The kinetic energy cutoff for plane wave expansions was set to 400 eV, and the reciprocal space was sampled by Γ-centered Monkhorst-Pack scheme with a grid of 3 × 3 × 1. The Methfessel-Paxton smearing of second order with a width of 0.2 eV was applied. The convergence criterion was 1×10^{-5} eV for solving the electronic wave function. All geometry optimizations of the initial state (IS), transition state (TS) and final state (FS) were considered to converge until the forces were smaller than 1×10^{-3} eV/Å.

The Ni, Pt, and Ni_3N slab models were constructed using the experimental lattice constants, which were 3.523 Å for *fcc* Ni, 3.924 Å for *fcc* Pt , and a = 4.622 Å and c = 4.306 Å for hexagonal Ni_3N.[7] The (4 × 4) Ni (111) and Pt (111) slab model of four layers were used for pure Ni and Pt, with the bottom two layers of atoms (Ni or Pt) fixed. For Ni_3N, a (2 × 2) Ni_3N (110) surface slab of 4 layers was built, with the bottom two layers fixed. We included at least 15 Å of vacuum in the z-direction to

minimize possible interactions between the replicated cells. The solvation effect was considered in calculation with an implicit solvation model as implemented in VASP and VASPsol, in which the effect of electrostatics, cavitation, and dispersion on the interaction between a solute and solvent was considered.[8]

The adsorption energy of hydrogen was calculated as follows:

$$E_{\text{adsorption}} = E_{\text{slab-H}} - (E_{\text{slab}} + 1/2E_{\text{H2}}) \quad \text{(S1)}$$

Zero-point energy (ZPE) and entropic corrections (TΔS) were included for calculating the Gibbs free energy correlations using the following equation:

$$\Delta G = \Delta E + (\text{ZPE} - \text{T}\Delta\text{S}) \quad \text{(S2)}$$

where the ZPE was calculated by summing over vibrational modes from frequency calculations:

$$ZPE = \sum_{i}^{\text{modes}} \frac{1}{2} h\nu_i \quad \text{(S3)}$$

We employed -0.202 eV as TS of H_2 gas at 298 K.[9] The TS for adsorbed species was set to zero. The transition state of water dissociation was predicted from the climbing image nudged elastic band (CI-NEB) method as implemented in the VASP-VTST code.[10] Six images were included in the CI-NEB calculation, which included four intermediate images together with the initial and the final images. The CI-NEB calculation was considered to be converged until the force was smaller than 1×10^{-3} eV/Å. Additional vibrational frequency calculations were carried out to confirm that the TS was a saddle point with only one imaginary frequency.

The atomic charge of surface atoms was estimated by employing the Bader Charge Analysis version 1.03.[11]

Reference

1. Y. Cong, B. Yi and Y. Song, *Nano Energy*, 2018, **44**, 288-303.

2. E. S. Davydova, S. Mukerjee, F. Jaouen and D. R. Dekel, *ACS Catal.*, 2018, **8**, 6665-6690.

3. G. Kresse, J. Furthmüller, Comput. *Mater. Sci.*,1996, **6**, 15-50.

4. G. Kresse, J. Hafner, Phys. Rev. B: Condens. *Matter Mater. Phys.*, 1994, **49**, 14251-14269.

5. G. Kresse, J. Hafner, Phys. Rev. B: Condens. *Matter Mater. Phys.*, 1993, **47**, 558-561.

6. J. P. Perdew, K. Burke, M. Ernzerhof, *Phys. Rev. Lett.*, 1996, **77**, 3865-3868.

7. A. Leineweber, H. Jacobs, S. Hull, *Inorg. Chem.*, 2011, **40**, 5818-5822.

8. K. Mathew, R. Sundararaman, K. Letchworth-Weaver, T. A. Arias, R. G. Hennig, *J. Chem. Phys.*, 2014, **140**, 084106.

9. *NIST Chemistry Webbook*, https://webbook.nist.gov/cgi/cbook.cgi?ID=C1333740 &Mask=1

10. G. Henkelman, B. P. Uberuaga, H. Jónsson, *J. Chem. Phys.*, 2000, **113**, 9901-9904.

11. M. Yu, D. R. Trinkle, *J. Chem. Phys*., 2011, **134**, 064111.

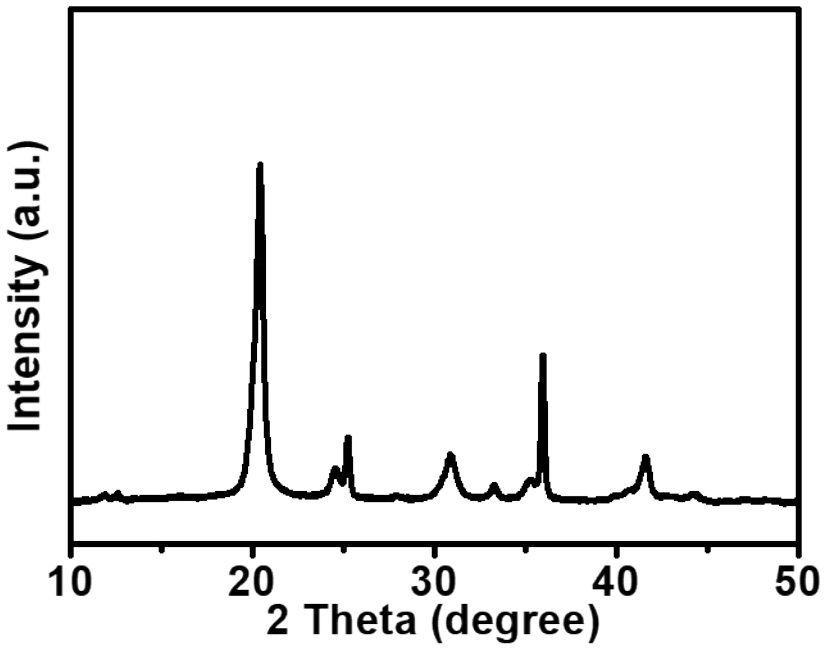

Fig. S1. XRD of Ni-CP from the first step solution reaction.

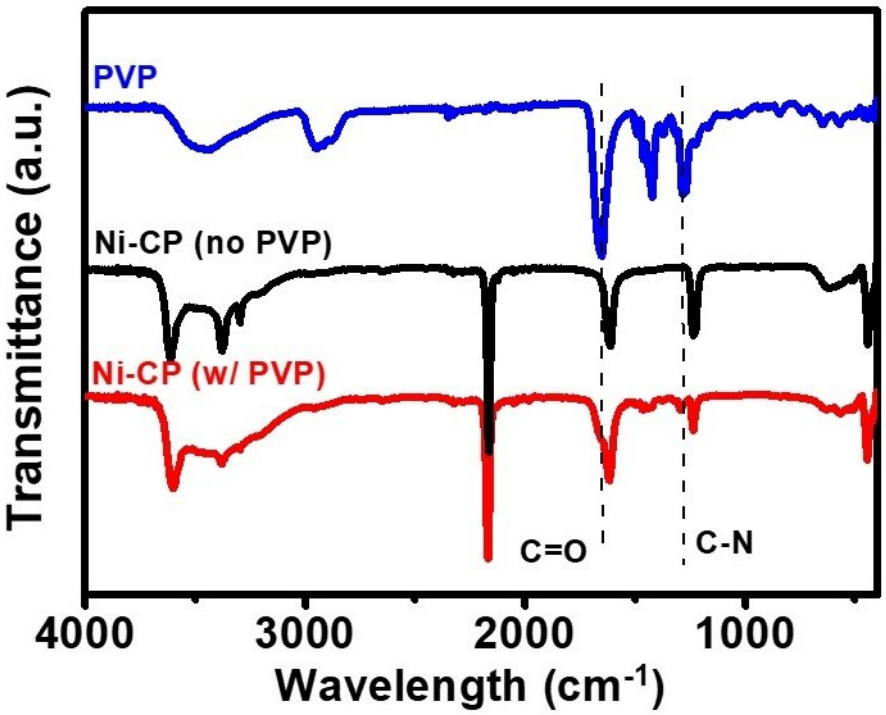

Fig. S2. FTIR spectra of PVP alone and Ni-CP prepared in the presence or absence of PVP.

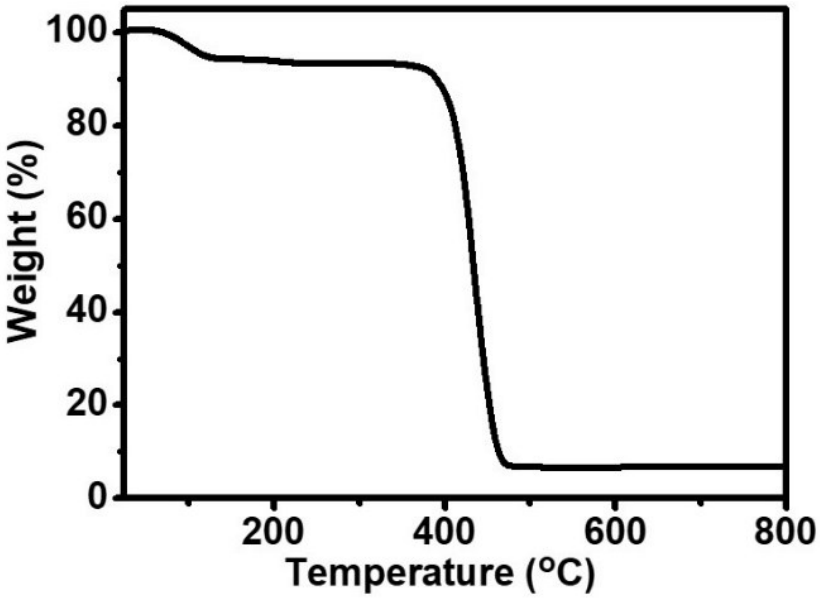

Fig. S3. TGA curve of PVP alone under N_2.

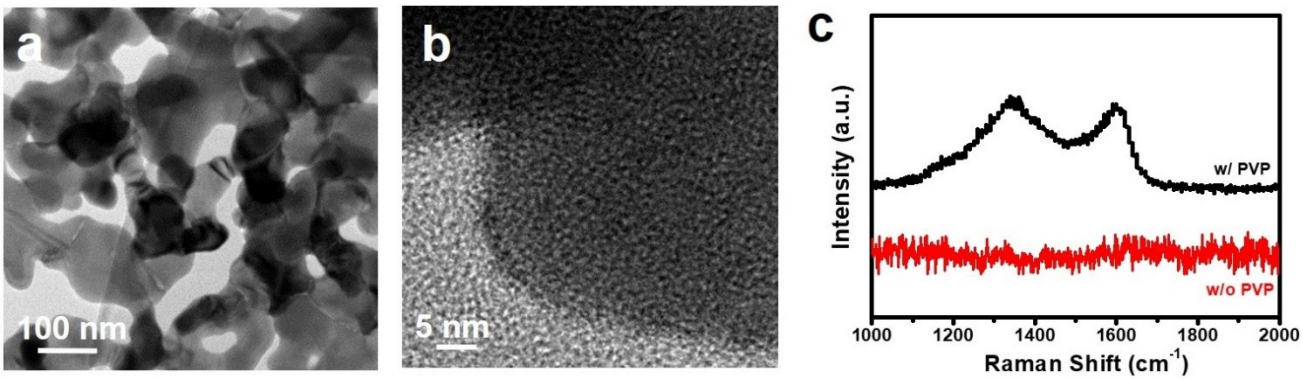

Fig. S4. (a,b) TEM images of Ni_3N prepared without PVP; (c) Raman spectra of Ni_3N samples prepared with or without PVP. These results confirm that surface-adsorbed PVP on Ni-CP is the precursor to the carbonaceous network observed in our np-Ni_3N.

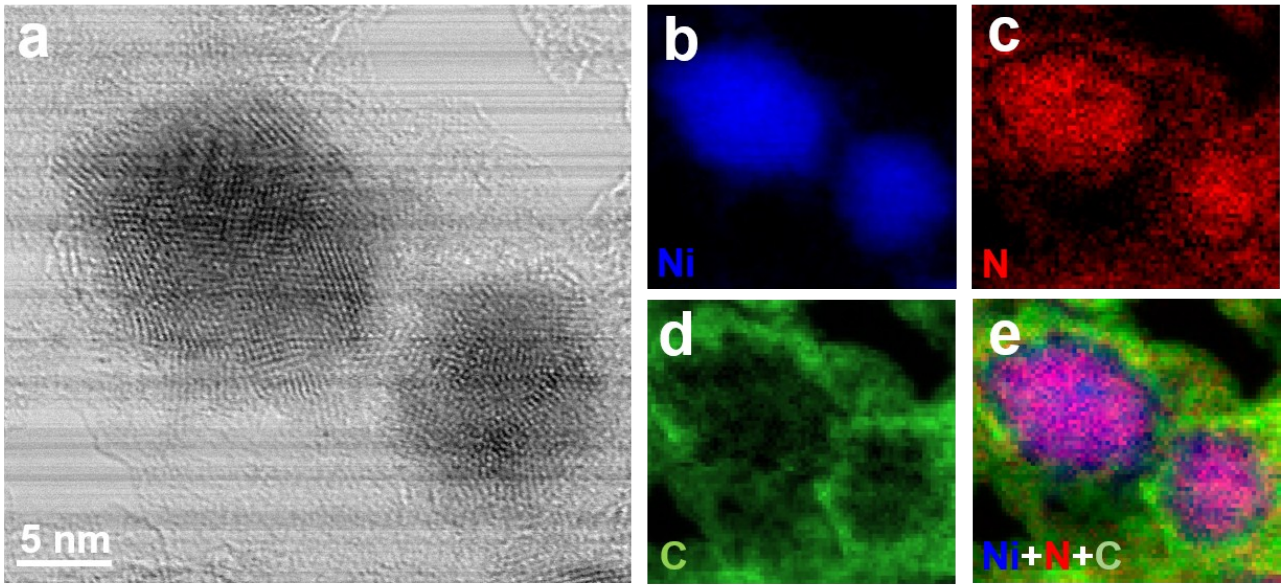

Fig. S5. (a) STEM image and (b-e) corresponding EDS mapping of np-Ni_3N.

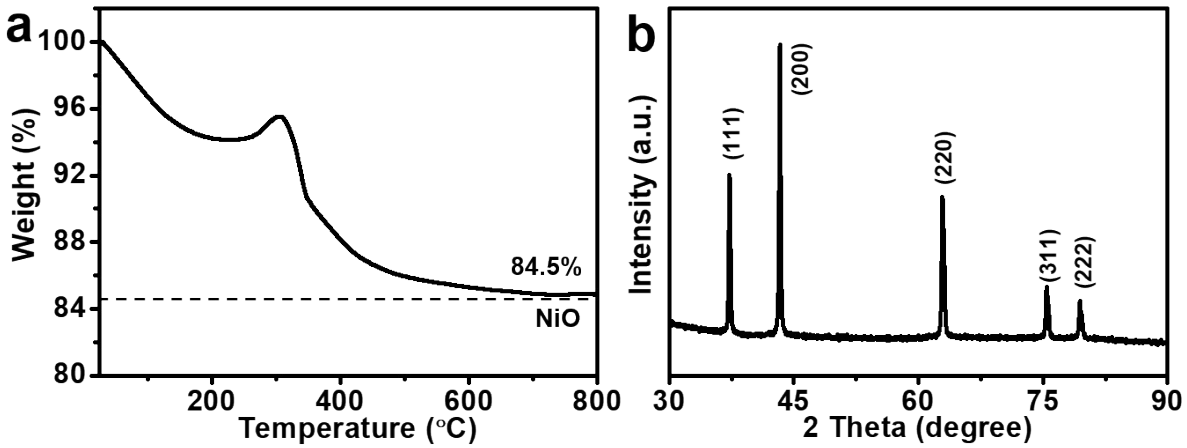

Fig. S6. (a) TGA of np-Ni_3N in air; (b) XRD of the residue after the TGA test showing it is composed of NiO.

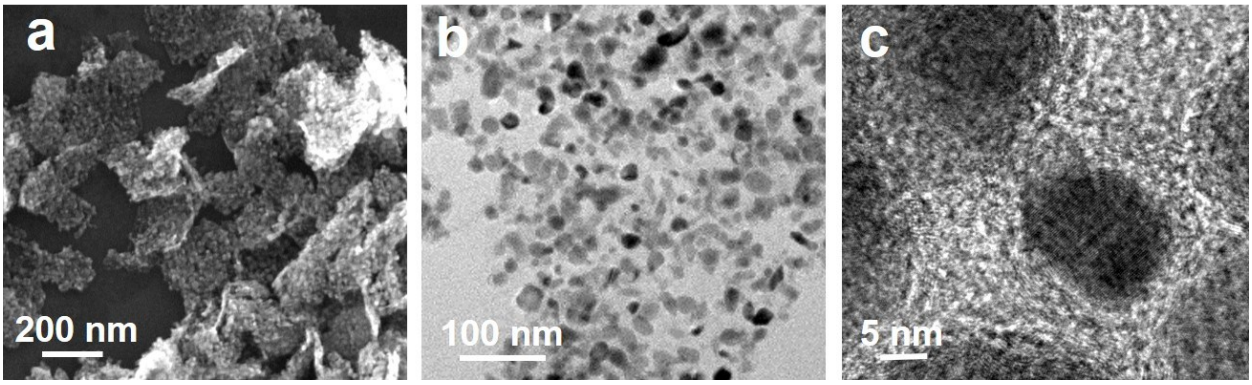

Fig. S7. (a) SEM image and (b,c) TEM images of np-Ni.

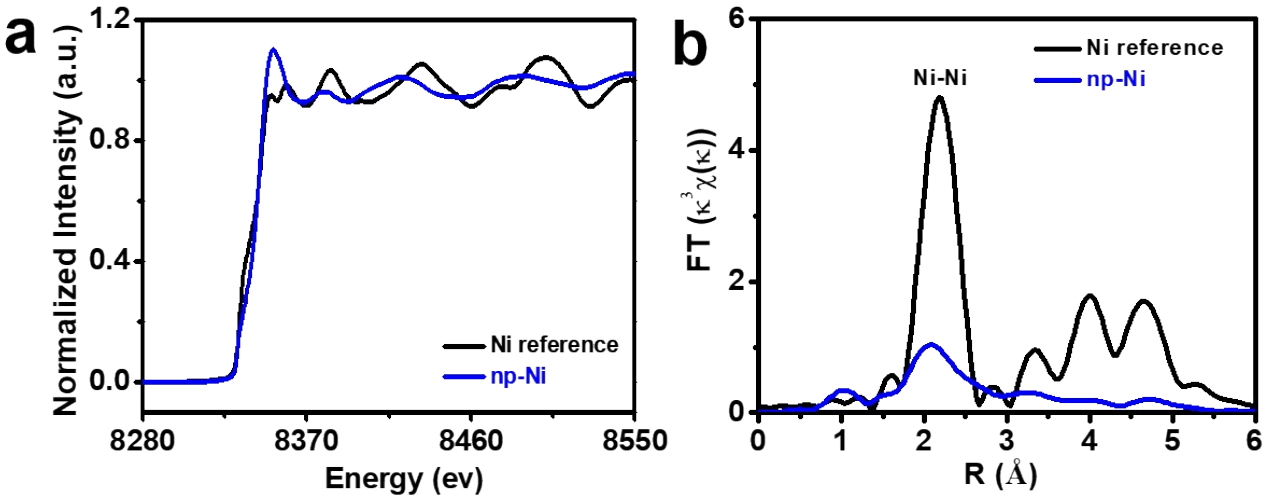

Fig. S8. (a) Ni K-edge XANES spectra of np-Ni and Ni foil; (b) corresponding EXAFS spectra from the Fourier transform of (a).

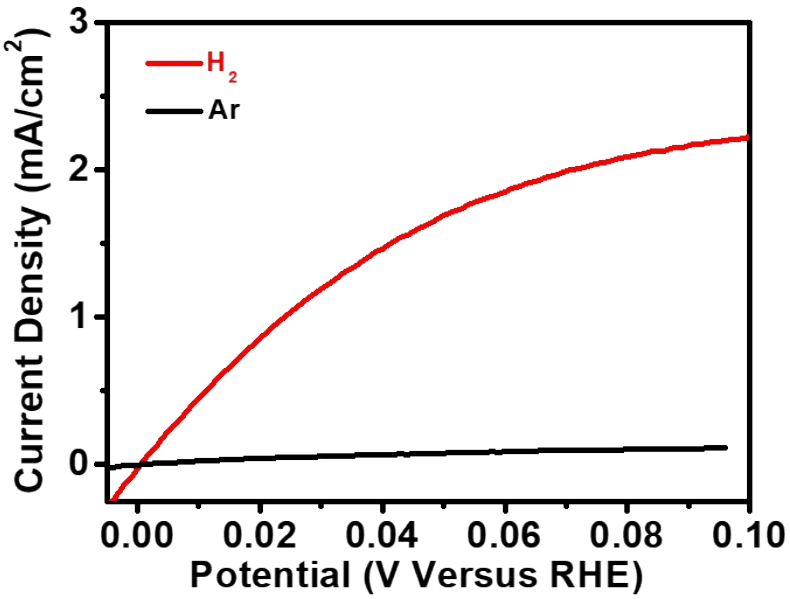

Fig. S9. Polarization curves of np-Ni_3N in (red) H_2 and (black) Ar-saturated 0.1 M KOH at 1600 rpm.

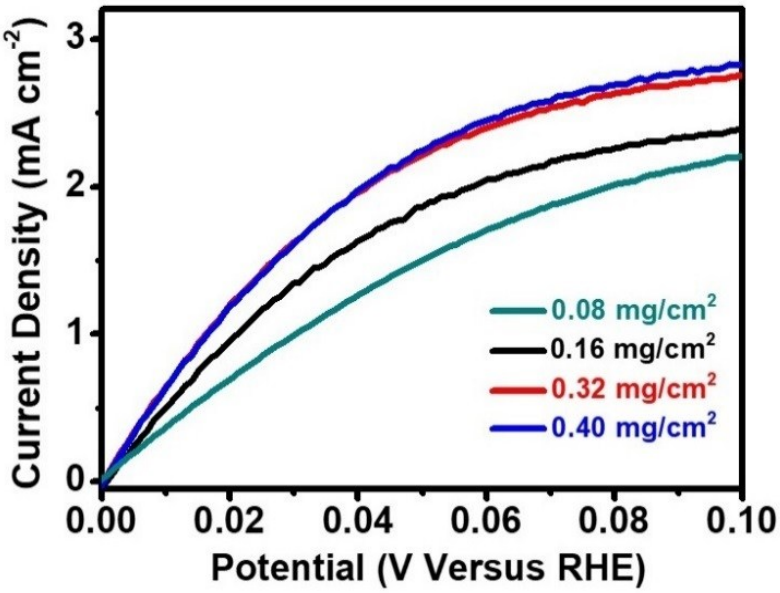

Fig. S10. HOR polarization curves of np-Ni_3N having different loading densities at 1600 rpm in H_2-saturated 0.1 M KOH.

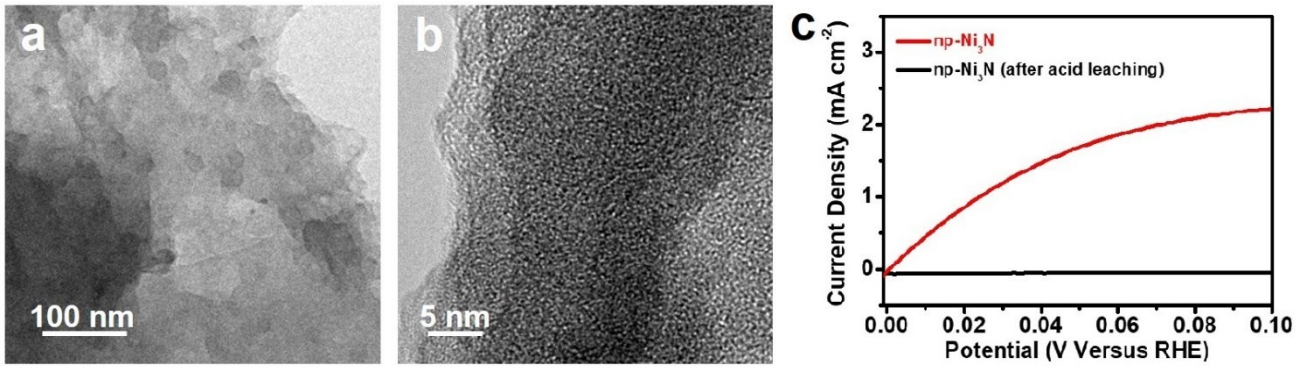

Fig. S11. (a,b) TEM images of np-Ni_3N after the acid leaching showing that Ni_3N nanoparticles are completely dissolved and only the carbonaceous network remains; (c) HOR polarization curves of as-prepared np-Ni_3N and np-Ni_3N after the acid leaching. These results confirm that Ni_3N is the active species for electrocatalytic HOR.

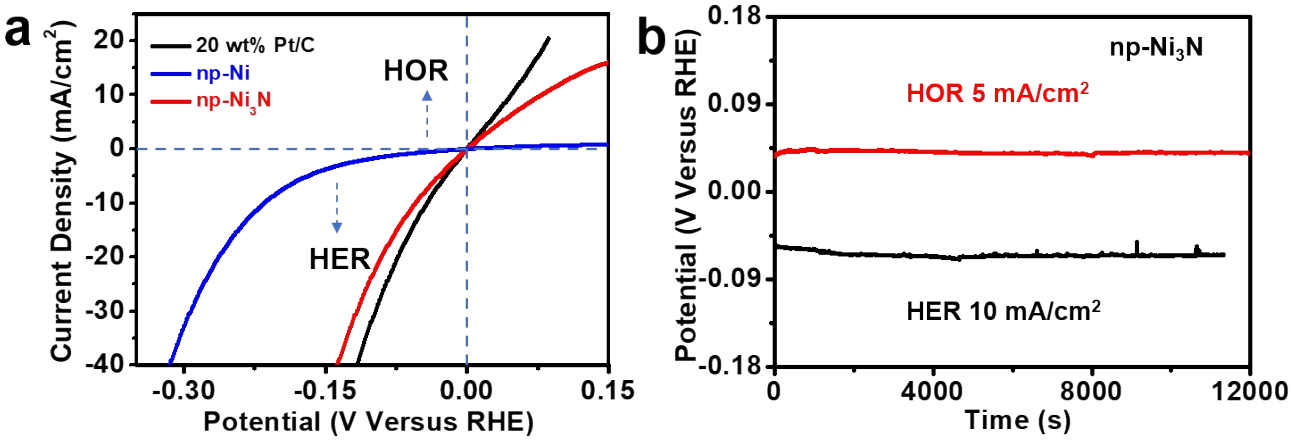

Fig. S12. (a) Polarization curves of np-Ni_3N, np-Ni and 20 wt% Pt/C loaded on the carbon fiber paper electrode for HOR and HER in 1 M KOH at room temperature; (b) chronopotentiometric stability of np-Ni_3N for HOR (at J = 5 mA/cm^2) and HER (at J = 10 mA/cm^2). The catalyst loading is 1 mg/cm^2 for np-Ni_3N and np-Ni, and 0.5 mg/cm^2 for Pt/C. Note that Teflon-treated carbon fiber paper can provide abundant gas-liquid-solid triple-phase boundaries for HOR. H_2 can be directly supplied from the atmosphere through the carbon fiber paper to reach the triple-phase boundary, and gets oxidized there. As a result, the measured current density on carbon fiber paper is much less limited by H_2 diffusion and better reflects the HOR kinetics. Its value is several times larger than that on RDE.

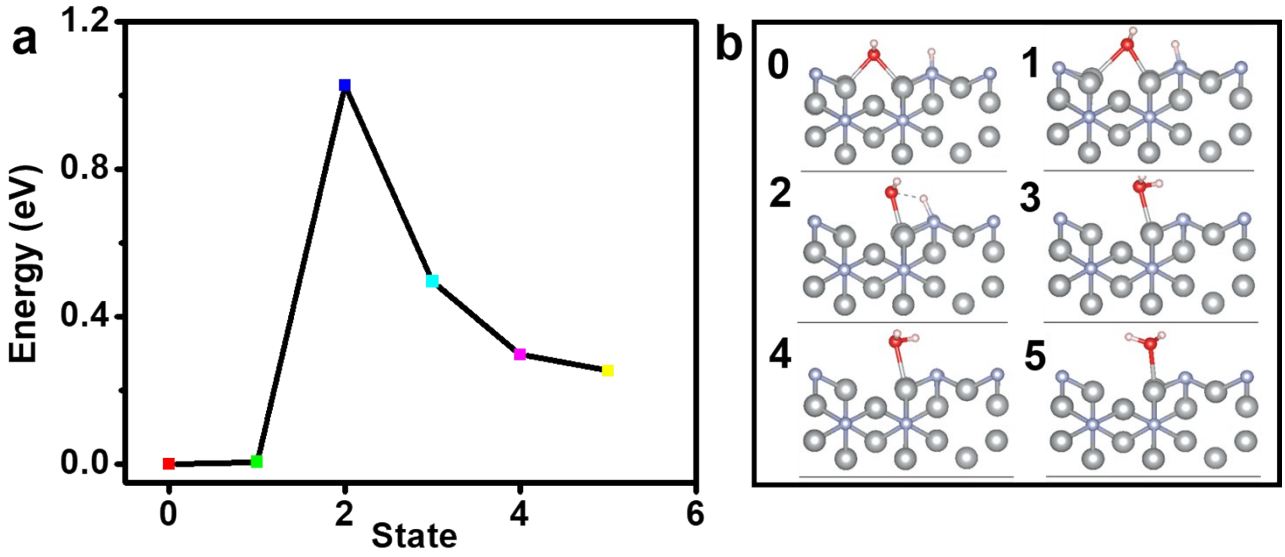

Fig. S13. (a) Reaction pathway for water formation on Ni_3N; (b) corresponding adsorption configurations of reaction intermediates along the reaction pathway. Color code: Ni (grey), N (light blue), H (white), O (red).

Supporting Table S1. Comparison of the alkaline HOR activity of our catalyst with literature results.

Electrocatalyst	Electrolyte	T (℃)	Loading (mg_{metal}/cm^2)	J_{mk} (A/g) @ η = 50 mV	J_{m0} (A/g)	Reference
np-Ni_3N	**0.1 M KOH**	**25**	**0.16**	**29.75**	**10.3**	**This work**
Ni/N-CNT	0.1 M KOH	RT	0.25	9.3	3.54	*Nat. Commun.* 2016, **7**, 10141.
Ni/CNT	0.1 M KOH	RT	0.25	1.9	0.98	*Nat. Commun.* 2016, **7**, 10141.
Ni	0.1 M KOH	RT	0.25	0.28	0.15	*Nat. Commun.* 2016, **7**, 10141.
50% Ni_9Mo_1/KB	0.1 M NaOH	25		-	4.5	*J. Mater. Chem. A* 2017, **5**, 24433.
$Ni_{0.95}Cu_{0.05}$/C			0.25		2.5	*J. Electroanal. Chem.* 2016, **783**, 146
Ni_3@h-$(BN)_1$/C-700NH_3	0.1 M NaOH	RT		-	3.3	*Chem. Sci.* 2017, **8**, 5728.

Supporting Table S2. Comparison of the alkaline HER activity of our catalyst with literature results.

Electrocatalysts	Electrolyte	Loading (mg/cm^2)	Overpotential (mV @ J = 10 mA/cm^2)	References
np-Ni_3N	**1 M KOH**	**0.16**	**68**	**This work**
np-Ni_3N (high-loading)	**1 M KOH**	**0.32**	**50**	**This work**
Co_2Ni_1N	1 M KOH	0.24	102.6	*ACS Appl. Mater. Interfaces* 2019, **11**, 8018.
NiMoN	1 M KOH	1.1	109	*Adv. Energy Mater.* 2016, **6**, 1600221.
NiCuN	1 M KOH	1.5	93	*Adv. Funct. Mater.* 2018, **28**, 1803278.
Fe-Ni_3C	1 M KOH	0.15	292	*Angew. Chem. Int. Ed.* 2017, ***56***, 12566.
Ni_2P/Fe_2P	1 M KOH	0.152	121	*Adv. Energy Mater.* 2018, **8**, 1800484.
Ni_3S_2	1 M KOH	1.6	223	*J. Am. Chem. Soc.* 2015, **137**, 14023.
NiS_2/MoS_2	1 M KOH	0.2	204	*ACS Catal.* 2017, **7**, 6179.
Ni_5P_4 /Ni foil	1 M KOH	3.5	150	*Angew. Chem. Int. Ed.* 2015, **54**, 12361.
Ni_3N nanosheets	1 M KOH	0.3	115	*J. Mater. Chem. A* 2017, **5**,9377.
Ni_3N-Co	1 M KOH	2.91	194	*Adv. Mater.* 2018, **30**, 1705516.
Ni_3FeN/RGO	1 M KOH	0.5	94	*ACS Nano* 2018, **12**, 245.
Ni_3N@CQDs	1 M KOH	0.18	69	*ACS Nano* 2018, **12**, 4148.
N-doped Ni_3S_2	1 M KOH	0.59	155	*Adv. Energy Mater.* 2018, **8**, 1703538.
Co@N-CNTs@rGO	1 M KOH	0.5	87	*Adv. Mater.* 2018, **30**, 1802011.
Holey-NCP	1 M KOH	1	58	*J. Am. Chem. Soc.* 2018, **140**, 5241.
Co-MoS_2 / BCCF-21	1 M KOH	2	48	*Adv. Mater.* 2018, **30**, 1801450.
CoP/NCNHP	1 M KOH	2	115	*J. Am. Chem. Soc.* 2018, **140**, 2610.
V-Co_4N	1 M KOH	-	37	*Angew. Chem. Int. Ed.* 2018, **57**, 5076.

Supporting Method 1: Calculation of the mass-specific kinetic current of np-Ni_3N

We first calculated the kinetic current density J_k at η = 50 mV by extrapolating the linear plot of $J^{-1} \sim \omega^{-1/2}$ (as depicted in the inset of Fig. 3b) to $\omega^{-1/2} = 0$. J_k corresponded to the reciprocal of the intercept (0.21 cm^2/mA) and was calculated to be 4.76 mA/cm^2. Subsequently, the mass-specific kinetic current was calculated as follows:

$$J_{mk} = \frac{J_k}{m} = \frac{4.76\ mA/cm^2}{0.16\ mg/cm^2} = 29.75\ A/g$$

where m is the loading density of np-Ni_3N.

Supporting Method 2: Calculation of the mass-specific exchange current of np-Ni_3N

The Butler–Volmer equation shows that:

$$J_k = J_0(e^{\frac{\alpha F}{RT}\eta} - e^{\frac{(\alpha-1)F}{RT}\eta})$$

where α is the transfer coefficient, F is the Faraday constant, R is the ideal gas constant, T is the temperature, and J_0 is the exchange current density. When η is sufficiently small, the Butler–Volmer equation is simplified to

$$J_k = J = \frac{J_0 F}{RT}\eta$$

In our experiment, the exchange current J_0 of np-Ni_3N was calculated from the linear fitting of the micro-polarization region around the equilibrium potential as shown below:

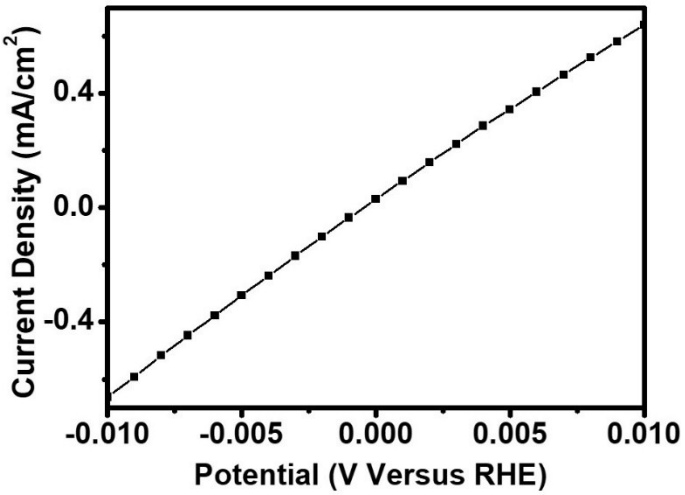

The fitting slope (b) was determined to be 64.3 mA/cm^2-V.

As a result, J_0 was calculated by:

$$J_0 = \frac{bRT}{F} = \frac{64.3\ mA/cm^2V \times 8.314\ J/Kmol \times 298\ K}{96485\ C/mol} = 1.65\ mA/cm^2$$

Jm_0 was calculated by:

$$J_{m0} = \frac{J_0}{m} = \frac{1.65\ mA/cm^2}{0.16\ mg/cm^2} = 10.3\ A/g$$